Applied Catalysis B: Environmental 255 (2019) 117776

Contents lists available at ScienceDirect

Applied Catalysis B: Environmental

journal homepage: www.elsevier.com/locate/apcatb

Enhancing formic acid dehydrogenation for hydrogen production with the metal/organic interface

Hongli Wang[a,1], Yue Chi[a,1], Dawei Gao[a], Zhili Wang[b,*], Cong Wang[a], Liying Wang[a], Minggang Wang[a], Daowen Cheng[a], Jingjing Zhang[a], Chen Wu[a], Zhankui Zhao[a,*]

[a] Key Laboratory of Advanced Structural Materials of Ministry of Education, College of Material Science and Engineering, Changchun University of Technology, Changchun 130012, China

[b] Key Laboratory of Automobile Materials Ministry of Education, Department of Materials Science and Engineering, Jilin University, Changchun 130022, China

ARTICLE INFO

Keywords:
Formic acid
Metal/organic interface
Hydrogen production
Heterogeneous catalyst

ABSTRACT

Ultrafine and well-dispersed CrPd nanoparticles are successfully immobilized on 3-aminopropyl triethoxysilane functionalized monochlortriazinyl β-cyclodextrin (M-β-CD-A) by a facile wet-chemical method. Benefiting from the strong metal/organic interfacial interactions between the CrPd nanoparticles and M-β-CD-A support, the $Cr_{0.4}Pd_{0.6}$/M-β-CD-A catalyst exhibits excellent catalytic activity towards formic acid dehydrogenation for hydrogen production, affording a high initial turn over frequency of 5771 mol H_2 mol Pd^{-1} h^{-1} without any additive at 323 K, which is much higher than those obtained for most of the reported noble metal catalysts under similar conditions. This work provides a promising lead for the design of efficient heterogeneous catalysts toward formic acid dehydrogenation for hydrogen production.

1. Introduction

Hydrogen (H_2) has attracted an increasing level of attention as an attractive and promising energy carrier for future applications because of its high energy density and environmentally friendly characteristics [1]. Safe and efficient storage and release of H_2 are well-known technological barriers toward a fuel cell based H_2 economy [1]. Formic acid (HCOOH, FA) has great potential as a safe and convenient H_2 storage material owing to its high energy density, high stability at room temperature, and non-toxicity [2,3]. The release of H_2 through FA dehydrogenation ($HCOOH(l) \rightarrow H_2(g) + CO_2(g)$, $\Delta G_{298K} = -35.0\ kJ\ mol^{-1}$) does not proceed spontaneously, and suitable catalysts must be needed [4]. Homogeneous catalysts have excellent catalytic activities for FA dehydrogenation but suffer from drawbacks such as separation issues and the use of organic solvents and additives [2,5–7]. Heterogeneous catalysts can avoid these drawbacks, and thus have received tremendous and increasing interest [8–10]. Until now, most of heterogeneous catalysts used for FA dehydrogenation are noble metals (such as Au, Pd and Pt) [8–11], which greatly hinders the practical application of FA as a H_2 storage material. To reduce the amount of noble metals used in FA dehydrogenation, intense research efforts have been focused on development of Pd-M (M are non-noble metals) catalysts [12,13]. However, the catalytic activities of these Pd-M catalysts are still far from desirable [13,14]. In this regard, the development of a heterogeneous catalyst containing non-noble metal with a high activity for FA dehydrogenation is highly required but remains a challenge.

It is generally acknowledged that the catalytic properties of heterogeneous catalysts are heavily dependent on the interactions between metal nanoparticles (NPs) and support [15,16]. The fabrication of metal/support interface has been emerging as an effective method to improve the catalytic properties of heterogeneous catalysts [17]. For example, Au NPs supported on CeO_2 exhibit improved catalytic activities for CO_2 reduction reaction as a result of the strong interfacial interactions between Au NPs and CeO_2 support [18]. Recently, it has been reported that reinforced catalytic effects from metal/support interfaces can greatly enhance the catalytic activities of heterogeneous catalysts for FA dehydrogenation [19–26]. For instance, Cao and co-workers have demonstrated that the catalytic activity of FA dehydrogenation can be significantly improved by the construction of the Au-ZrO_2 interface [19]. So far, the application of interfacial interactions between the metal NPs and support for enhancing FA dehydrogenation activity are mainly focused on metal/metal [27], metal/oxide and metal/carbon interfaces [19,20,28–31]. Recently, experimental and theoretical studies revealed that metal/organic interface can modify the

* Corresponding authors.
E-mail addresses: zhiliwang@jlu.edu.cn (Z. Wang), zhaozk@ccut.edu.cn (Z. Zhao).
[1] These authors contributed equally to this work.

https://doi.org/10.1016/j.apcatb.2019.117776
Received 30 January 2019; Received in revised form 30 April 2019; Accepted 24 May 2019
Available online 25 May 2019
0926-3373/

catalytic performance of heterogeneous catalysts for various reactions [32–36]. For example, Zheng and co-workers have demonstrated that ethylenediamine/Pt interface can promote the selectivity in the hydrogenation of nitro aromatics due to the interfacial electronic effect [35]. However, to the best of our knowledge, the application of metal/organic interface to improve the catalytic activity of FA dehydrogenation for H_2 production has not been reported.

Herein, for the first time, we report a wet-chemical method to create high performance catalytic metal/organic interface towards FA dehydrogenation for H_2 production by growing CrPd NPs on 3-aminopropyl triethoxysilane (APTES) functionalized monochlortriazinyl β-cyclodextrin (M-β-CD-A). The M-β-CD, a green, nontoxic, and cyclic oligosaccharide consisting of seven glucose units linked via α-1-4 glycosidic bonds, was chosen as a support because of its potential ability to form strong interactions between the metal NPs and M-β-CD by a guest-host complex behavior, which can improve the catalytic properties of the metal NPs [37,38]. Due to the strong interfacial interactions between the CrPd NPs and M-β-CD-A support, the $Cr_{0.4}Pd_{0.6}$ NPs supported on M-β-CD-A ($Cr_{0.4}Pd_{0.6}$/M-β-CD-A) exhibit excellent catalytic activities for FA dehydrogenation, giving an initial turn over frequency (TOF) as high as 5771 mol H_2 mol Pd^{-1} h^{-1} without any additive at 323 K, which is much higher than those obtained for most of the reported heterogeneous catalysts for FA dehydrogenation under similar conditions.

2. Experimental

2.1. Chemicals

Palladium chloride ($PdCl_2$, Pd ≥ 59%), sodium chloride (NaCl, ≥ 99.5%), chromium nitrate nonahydrate ($Cr(NO_3)_3{\cdot}9H_2O$, ≥ 99%), M-β-CD (≥ 75%), Vulcan XC-72 carbon (C), and sodium formate (HCOONa, ≥ 99.5%) were purchased from Sinopharm Chemical Reagent Co., Ltd. FA (≥ 96%), sodium borohydride ($NaBH_4$, ≥ 98%), aluminum oxide (Al_2O_3, ≥ 99.0%), silicon dioxide (SiO_2, ≥ 99.5%), zirconium dioxide (ZrO_2, ≥ 99.0%), titanium oxide (TiO_2, ≥ 99.0%), cerium oxide (CeO_2, ≥ 99.99%), APTES (≥ 98%), and ethanol (CH_3CH_2OH, ≥ 99.7%) were obtained from Aladdin Chemistry Co., Ltd. De-ionized water with the specific resistance of 18.2 MΩ·cm was obtained by reversed osmosis followed by ion-exchange and filtration.

2.2. Synthesis of catalysts

All the catalysts were prepared by a wet-chemical method. Na_2PdCl_4 aqueous solution (0.025 M) was prepared previously by dissolving NaCl (1.5 mmol) and $PdCl_2$ (0.75 mmol) into 30.0 mL H_2O with magnetic stirring for 3 h. Typically, for the preparation of $Cr_{0.4}Pd_{0.6}$/M-β-CD-A, 40 mg M-β-CD and 0.4 mL APTES were added into 10.0 mL distilled water with ultra-sonication for 40 min, and then an aqueous solution contained $Cr(NO_3)_3{\cdot}9H_2O$ (0.02 M, 2.0 mL) and Na_2PdCl_4 (0.025 M, 2.4 mL) was added into the above suspension with magnetic stirring for 3 h. Then the resulting mixture was reduced by $NaBH_4$ (40.5 mg) and stirred for 30 min. The obtained catalyst was centrifuged and washed three times with distilled water.

For comparison, $Cr_{0.4}Pd_{0.6}$-A, $Cr_{0.4}Pd_{0.6}$/M-β-CD, and free $Cr_{0.4}Pd_{0.6}$ NPs were prepared as the similar method mentioned above. In addition, $Cr_{0.4}Pd_{0.6}$ NPs supported on C and various oxides (TiO_2, ZrO_2, SiO_2, CeO_2 and Al_2O_3) were prepared as the same method mentioned above. $Cr_{0.4}Pd_{0.6}$ NPs supported on various APTES-treated supports (C, TiO_2, ZrO_2, SiO_2, CeO_2 and Al_2O_3) were also prepared as the above method, except adding 0.4 mL APTES to the supports. To study the effect of molar ratio of Cr/Pd on the activity of FA dehydrogenation, Cr_xPd_{1-x}/M-β-CD-A [x = 0, 0.2, 0.4, 0.6, 0.8, and 1.0 obtained from the equation of $x = n_{Cr}/(n_{Cr}+n_{Pd})$] were prepared by the same method except altering the dosage of $Cr(NO_3)_3{\cdot}9H_2O$ and Na_2PdCl_4.

2.3. Catalyst characterization

The detailed microstructures and compositions of catalysts were examined using a transmission electron microscope (TEM, FEI-Talos-F200S). The infrared spectroscopy (IR) spectra were recorded on a Thermo IS50. Fourier transform infrared spectroscopy (FT-IR) in the wave number range from 500 to 4000 cm^{-1}. Inductively coupled plasma-optical emission spectroscopy (ICP-OES) measurements were performed on a Thermo Jarrell Ash (TJA) Atom scan Advantage instrument. X-ray diffraction (XRD) measurements were performed on a Rigaku RINT-2000 X-ray generator with Cu Kα radiation (λ = 1.54056 Å). X-ray photoelectron spectroscopy (XPS) spectra were acquired with an ESCALABMKLL (Vacuum Generators) spectrometer using Al Kα X-rays. Detailed analyses for CO_2, H_2, and CO were performed on gas chromatography (GC-7900) with thermal conductivity detector (TCD) and flame ionization detector (FID)-Methanator (detection limit: ~10 ppm for CO).

2.4. H_2 generation from FA dehydrogenation

The as-prepared catalyst was kept in a round-bottom flask with two necks, one neck was connected to a gas burette, and the other was connected to a pressure-equalization funnel to introduce FA aqueous solution (1.0 M, 5.0 mL). The reaction started once the FA solution was added into the flask with magnetic stirring (600 r/min). The generated gas was monitored using the gas burette. The reactions were carried out at different temperatures (303, 313, 323, and 333 K) under ambient atmosphere.

2.5. Calculation methods

The initial TOF was calculated using the following equation:

$$TOF = \frac{P_{atm} V_{H_2}/RT}{n_{Pd} t} \quad (1)$$

Where P_{atm} is the atmospheric pressure, V_{H2} is the volume of the generated H_2 when the conversion reaches 20% or 50%, R is the universal gas constant, T is the room temperature (298 K), n_{Pd} is the molar number of Pd, and t is the reaction time when the conversion reaches 20% or 50%.

The relationship between temperatures and initial TOF values was followed Arrhenius behavior. The Arrhenius' reaction rate equation can be calculated as follows:

$$\ln TOF = \ln A - E_a/RT \quad (2)$$

Where A is the reaction constant.

3. Results and discussion

3.1. Synthesis and characterization of catalysts

The CrPd NPs immobilized by M-β-CD-A were prepared by a facile wet-chemical method under ambient atmosphere and room temperature. Briefly, for the synthesis of $Cr_{0.4}Pd_{0.6}$/M-β-CD-A, 0.4 mL APTES was mixed with 10.0 mL aqueous solution containing 40.0 mg M-β-CD by sonicating for 40 min at room temperature to form a uniform transparent M-β-CD-A solution. Then 2.0 mL $Cr(NO_3)_3{\cdot}9H_2O$ (0.02 M) and 2.4 mL Na_2PdCl_4 (0.025 M) aqueous solutions were added into the M-β-CD-A solution with magnetic stirring for 3 h. Finally, 40.5 mg $NaBH_4$ was added into the above mixture solution under magnetic stirring for 30 min, and the $Cr_{0.4}Pd_{0.6}$/M-β-CD-A catalyst can be obtained. Fig. 1a shows the FT-IR spectra of M-β-CD and $Cr_{0.4}Pd_{0.6}$/M-β-CD-A catalyst. For M-β-CD, the broad peak around 3416 cm^{-1} corresponds to the −OH stretching vibration, the band at 2938 cm^{-1} related to C–H stretching vibration [39], the vibration peaks around

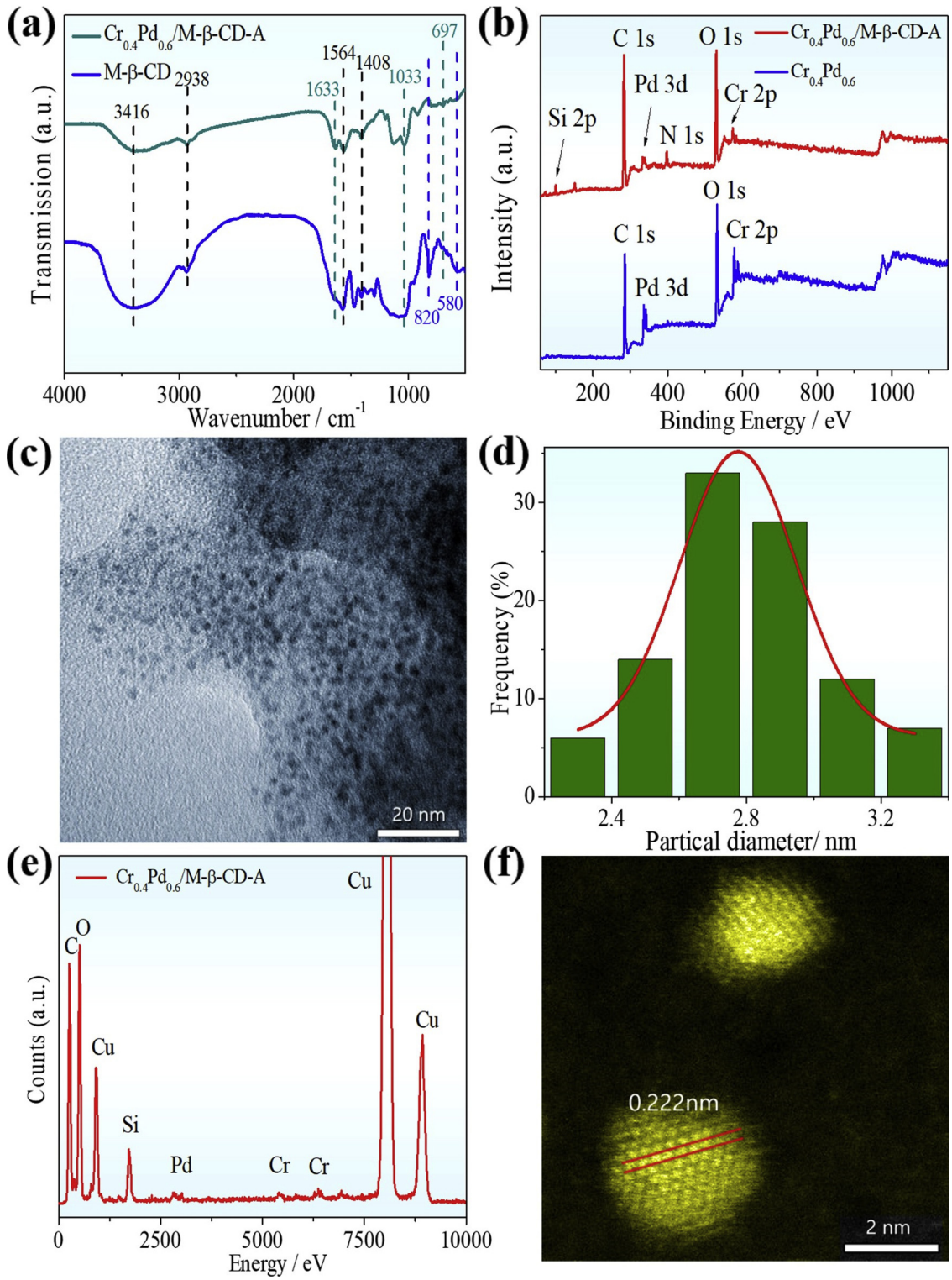

Fig. 1. (a) IR spectra of $Cr_{0.4}Pd_{0.6}$/M-β-CD-A and M-β-CD. (b) XPS spectra of $Cr_{0.4}Pd_{0.6}$/M-β-CD-A and $Cr_{0.4}Pd_{0.6}$ NPs. (c) TEM image, (d) particle size distribution, (e) EDX spectrum, and (f) high-resolution TEM image of $Cr_{0.4}Pd_{0.6}$/M-β-CD-A.

1625–1400 cm^{-1} assigned totriazinyl groups [40], and the bands at 820 cm^{-1} and 580 cm^{-1} are assigned to C-Cl groups [41]. For $Cr_{0.4}Pd_{0.6}$/M-β-CD-A catalyst, the peaks correspond to C-Cl groups in the M-β-CD disappeared, and three new bands at 1633 and 1033/697 cm^{-1} correspond to the N—H stretching vibrations [42] and Si-O groups [43], respectively, are observed, confirming C-Cl substituted by APTES to form M-β-CD-A in the $Cr_{0.4}Pd_{0.6}$/M-β-CD-A catalyst. To further confirm the presence of APTES and M-β-CD in $Cr_{0.4}Pd_{0.6}$/M-β-CD-A catalyst, XPS analyses have been applied. As shown in Fig. 1b, in addition to peaks of Pd, Cr, C, and O, the N peak at 399.3 eV and Si peak at 102.1 eV are observed for the $Cr_{0.4}Pd_{0.6}$/M-β-CD-A catalyst, whereas such N and Si peaks do not exist in $Cr_{0.4}Pd_{0.6}$ NPs, further suggesting that the APTES and M-β-CD have been successfully decorated into $Cr_{0.4}Pd_{0.6}$/M-β-CD-A catalyst. In addition, the Pd 3d and Cr 2p XPS spectra of the $Cr_{0.4}Pd_{0.6}$/M-β-CD-A (Fig. S1) show that the surface Pd is mainly in the metallic state, whereas most of Cr on the catalyst surface

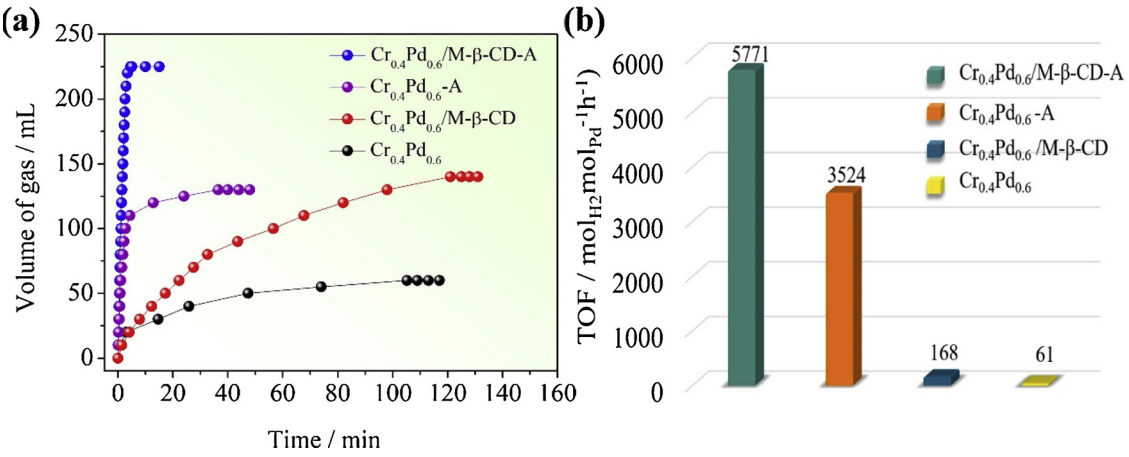

Fig. 2. (a) Gas generation from the dehydrogenation of FA (1.0 M, 5.0 mL) versus time in the presence of $Cr_{0.4}Pd_{0.6}$/M-β-CD-A, $Cr_{0.4}Pd_{0.6}$-A, $Cr_{0.4}Pd_{0.6}$/M-β-CD and $Cr_{0.4}Pd_{0.6}$ NPs (n_{Pd}/n_{FA} = 0.005). (b) The initial TOF values of different catalysts.

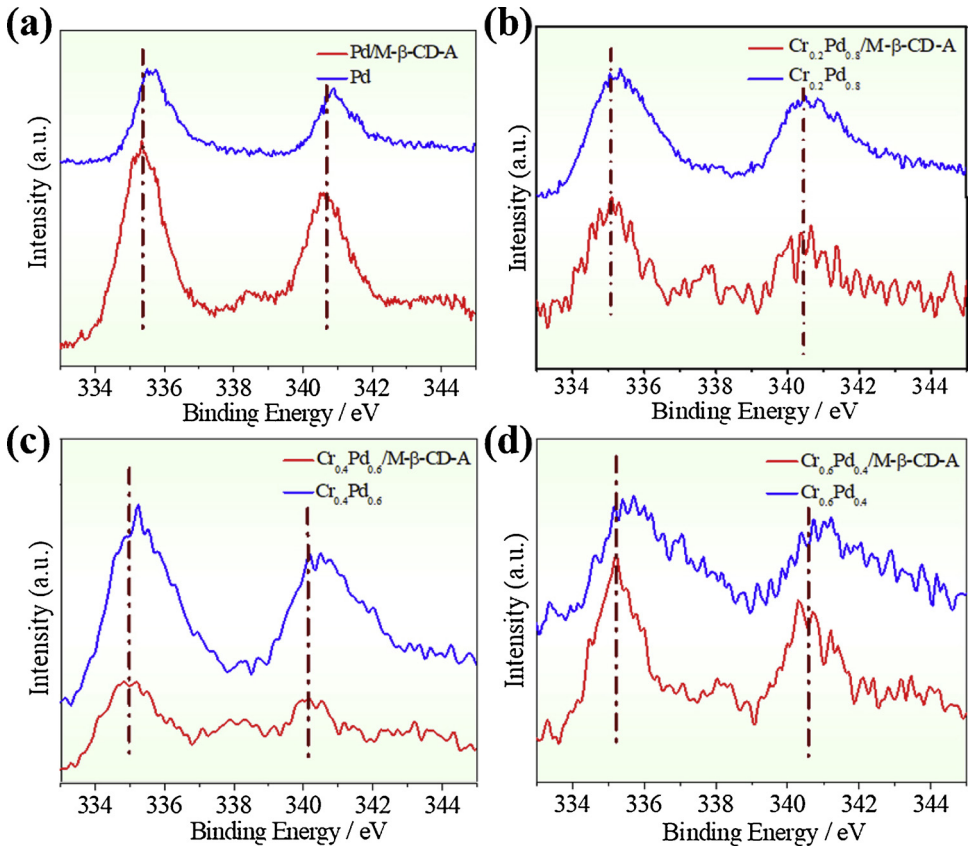

Fig. 3. The high-resolution XPS spectra of Pd 3d for Cr_xPd_{1-x}/M-β-CD-A and free Cr_xPd_{1-x} NPs (x = 0, 0.2, 0.4, 0.6).

is in the oxidized state (due to the occurrence of surface oxidation of Cr during sample preparing for XPS) [44].

Fig. 1c shows a typical TEM image of the $Cr_{0.4}Pd_{0.6}$/M-β-CD-A catalyst. It can be seen that the CrPd NPs are highly dispersed on M-β-CD-A with an average size of ˜2.8 nm (Fig. 1d). Energy-dispersive X-ray spectroscopy (EDX) result indicates the existence of C, O, Si, Cr and Pd elements (Fig. 1e). The molar ratio of Cr:Pd is quantitatively determined to be 0.43:0.57 by ICP-OES (Table S1), which agrees very well with the designed ratio. On the contrary, the $Cr_{0.4}Pd_{0.6}$ NPs prepared without support are highly agglomerated and have a larger average size of ˜4.8 nm (Fig. S2a). Without APTES, the $Cr_{0.4}Pd_{0.6}$ NPs supported on M-β-CD ($Cr_{0.4}Pd_{0.6}$/M-β-CD) are severely aggregated with an average size of ˜3.8 nm (Fig. S2b). Moreover, without M-β-CD support, the APTES-treated $Cr_{0.4}Pd_{0.6}$ NPs ($Cr_{0.4}Pd_{0.6}$-A) show slight aggregation with an average size of 3.1 nm (Fig. S2c). The high-resolution TEM (HRTEM) image of $Cr_{0.4}Pd_{0.6}$/M-β-CD-A (Fig. 1f) reveals the crystalline nature of $Cr_{0.4}Pd_{0.6}$ NPs, and the lattice spacing is measured to be 0.222 nm, which is smaller than that of the (111) plane of face-centered cubic Pd (0.224 nm, JCPDS file: 65-2867) [45], suggesting the reduction of the crystal lattice induced by alloying Cr with Pd structure [46]. The XRD pattern of $Cr_{0.4}Pd_{0.6}$/A-M-β-CD shows that a broad diffraction peak of (111) is located between the characteristic peaks of Pd (JCPDS file: 65-2867) and Cr (JCPDS file: 88-2323) (Fig. S3) [47], demonstrating that the $Cr_{0.4}Pd_{0.6}$ NPs are formed as alloy structures, and this is consistent with the HRTEM result. Unfortunately, due to the ultrafine size of the $Cr_{0.4}Pd_{0.6}$ NPs in $Cr_{0.4}Pd_{0.6}$/A-M-β-CD, it is difficult to

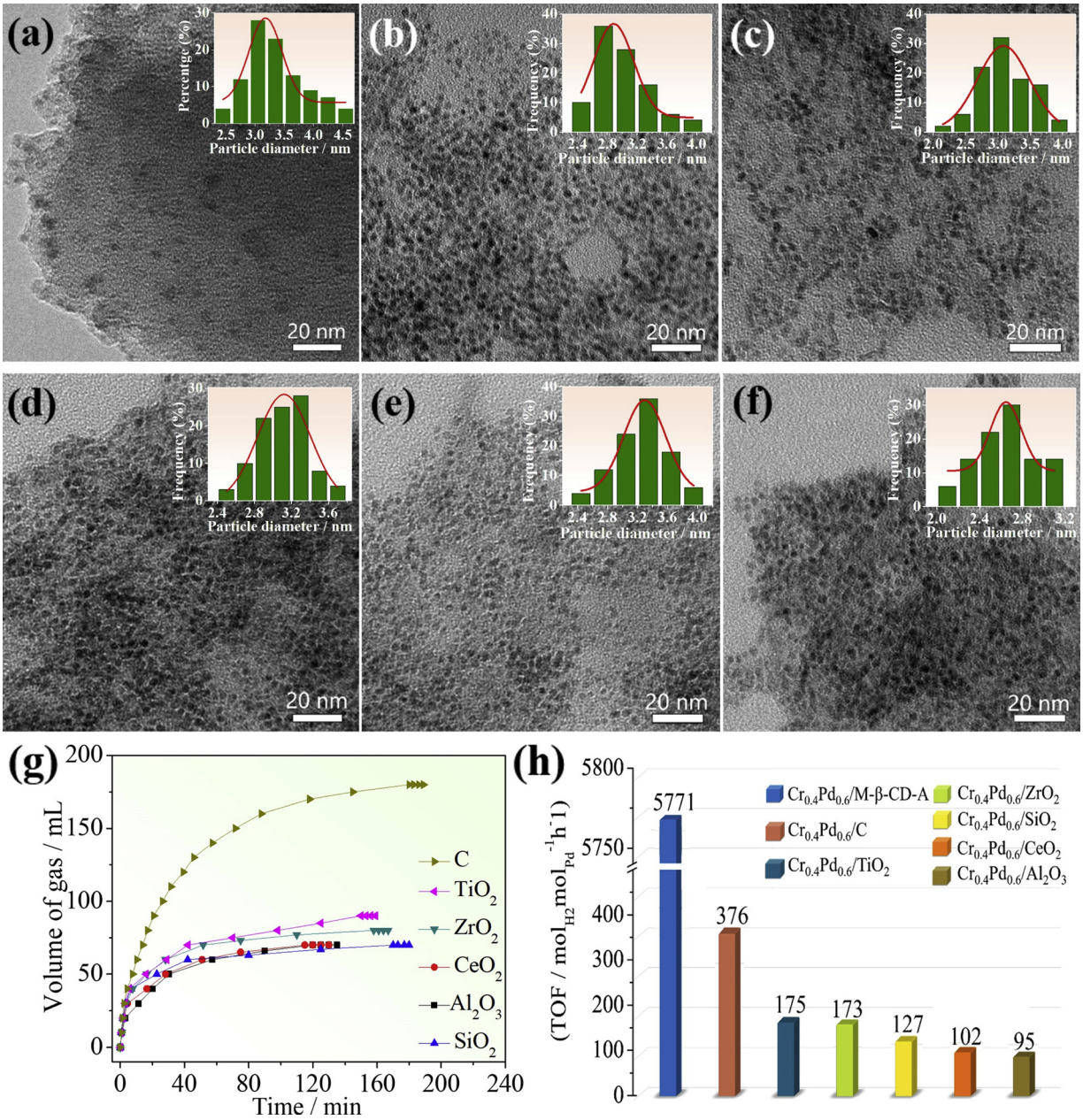

Fig. 4. TEM images and particle size distributions of (a) $Cr_{0.4}Pd_{0.6}$/C, (b) $Cr_{0.4}Pd_{0.6}/TiO_2$, (c) $Cr_{0.4}Pd_{0.6}/ZrO_2$, (d) $Cr_{0.4}Pd_{0.6}/SiO_2$, (e) $Cr_{0.4}Pd_{0.6}/CeO_2$ and (f) $Cr_{0.4}Pd_{0.6}/Al_2O_3$. (g) Gas generation from the dehydrogenation of FA (1.0 M, 5.0 mL) versus time catalyzed by $Cr_{0.4}Pd_{0.6}$ NPs supported on different supports (n_{Pd}/n_{FA} = 0.005). (h) Initial TOF values of different catalysts.

observe the alloy structure in EDX mapping images (Fig. S4). The smaller particle size and the better dispersion in the $Cr_{0.4}Pd_{0.6}$/M-β-CD-A suggest that the M-β-CD-A plays a key rule for the control of size and distribution of CrPd NPs, which can be explained as follows: after treating with APTES, the M-β-CD-A surface has abundant negatively-charged -NH_2 groups, which are prone to adsorb Pd^{2+} and Cr^{3+} ions as the initial nucleation sites through the charge interactions, and thus the M-β-CD-A can anchor the CrPd NPs without aggregation and control their sizes [48]. The drastic size and distribution differences also suggest the existence of strong interfacial interactions between the CrPd NPs and M-β-CD-A through the metal/organic interface.

3.2. Catalytic activities of catalysts for FA dehydrogenation

The activity of the as-prepared $Cr_{0.4}Pd_{0.6}$/M-β-CD-A catalyst towards FA dehydrogenation for H_2 production at 323 K under ambient atmosphere was evaluated in a typical water-filled graduated buret system and compared with $Cr_{0.4}Pd_{0.6}$ NPs, $Cr_{0.4}Pd_{0.6}$/M-β-CD, and $Cr_{0.4}Pd_{0.6}$-A catalysts (Fig. 2). It can be seen that the $Cr_{0.4}Pd_{0.6}$/M-β-CD-A catalyst exhibits the highest catalytic activity among all the catalysts, with which 225 mL of gas can be released within 4.5 min, corresponding to a conversion of 100%. Moreover, only the H_2 and CO_2 but no CO (detection limit: ≈10 ppm for CO) has been detected by GC (Fig. S5 and Fig. S6), reflecting the complete decomposition of FA into H_2 and CO_2 catalyzed by $Cr_{0.4}Pd_{0.6}$/M-β-CD-A catalyst. In contrast, only 60 mL of gas can be released within 105 min in the presence of $Cr_{0.4}Pd_{0.6}$ NPs, corresponding to a conversion of 27%. In addition, both $Cr_{0.4}Pd_{0.6}$-A and $Cr_{0.4}Pd_{0.6}$/M-β-CD catalysts show much lower activities than that of $Cr_{0.4}Pd_{0.6}$/M-β-CD-A catalyst, giving the FA conversions of 58% and 62% after 37 and 120 min, respectively. The $Cr_{0.4}Pd_{0.6}$/M-β-CD-A catalyst affords an extraordinary high initial TOF (Eq. 1) of 5771 mol H_2 mol Pd^{-1} h^{-1} at 323 K, which is 94.6, 34.4, and

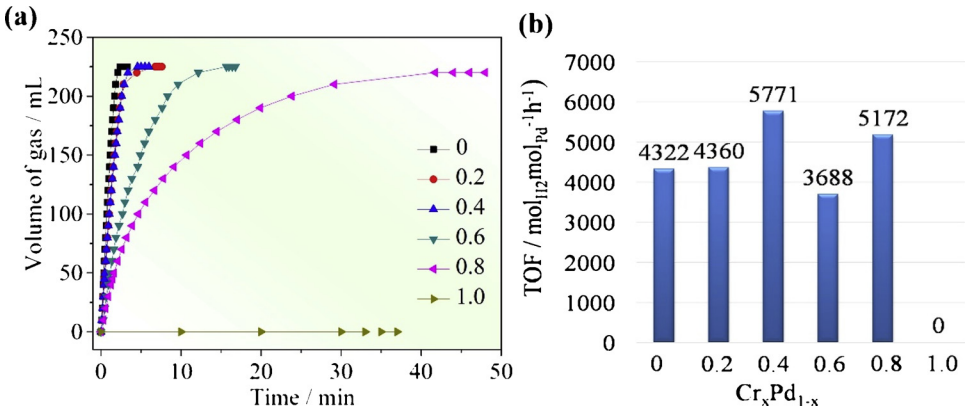

Fig. 5. (a) Gas generation from the dehydrogenation of FA (1.0 M, 5.0 mL) versus time in the presence of Cr_xPd_{1-x}/M-β-CD-A (x = 0, 0.2, 0.4, 0.6, 0.8, and 1.0) at 323 K under ambient atmosphere. (b) Initial TOF values with different Cr:Pd ratios.

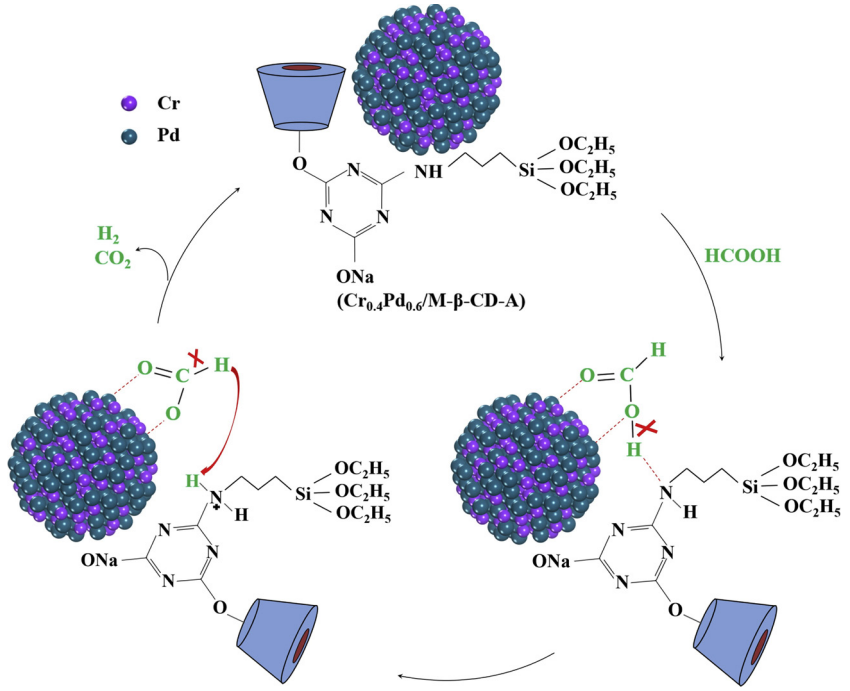

Fig. 6. Possible mechanism of FA dehydrogenation catalyzed by $Cr_{0.4}Pd_{0.6}$/M-β-CD-A.

1.6 times higher than that of the $Cr_{0.4}Pd_{0.6}$ NPs, $Cr_{0.4}Pd_{0.6}$/M-β-CD and $Cr_{0.4}Pd_{0.6}$-A catalysts, respectively (Fig. 2b). It is worth noting that this initial TOF value represents one of the highest activities ever reported for FA dehydrogenation without any additive [12,29,44,49–52], and even exceeds most of values obtained with additives and under elevated temperatures (Table S2) [53–59].

Based on the above results, it can be concluded that the strong interfacial interactions between the CrPd NPs and M-β-CD-A play an important role on the FA dehydrogenation activity. To study the effect of interfacial interactions on the electronic structure of Pd (the crucial active element for the FA dehydrogenation) and Cr [12], XPS measurements were performed on the electronic states of Pd and Cr for free Cr_xPd_{1-x} NPs and Cr_xPd_{1-x}/M-β-CD-A ($0 \le x \le 1.0$) catalysts. The binding energies of Pd $3d_{5/2}$ (Fig. 3) and Cr $2p_{3/2}$ (Fig. S7) in Cr_xPd_{1-x}/M-β-CD-A catalysts are shifted to lower values than those in free Cr_xPd_{1-x} NPs, respectively, suggesting that the interfacial interactions between CrPd NPs and M-β-CD-A support are strong, leading to electrons transfer from M-β-CD-A to CrPd NPs through the metal/organic interfaces between CrPd and M-β-CD-A [60]. It should be noted that the Pd 3d peaks in $Cr_{0.8}Pd_{0.2}$/M-β-CD-A and $Cr_{0.8}Pd_{0.2}$ NPs and the Cr 2p peaks in $Cr_{0.2}Pd_{0.8}$/M-β-CD-A and $Cr_{0.2}Pd_{0.8}$ NPs are not obvious due to their low element contents (Fig. S8). In addition, the binding energy of Pd 3d in $Cr_{0.4}Pd_{0.6}$/M-β-CD-A is shifted to lower value relative to that in Pd/M-β-CD-A (Fig. S9), demonstrating that the charge transfer between Pd and Cr occurred after alloying Pd with Cr [12]. Previous studies have shown that the electron-rich Pd surface can promote the rate determining of C–H dissociation of the Pd-formate intermediate to produce H_2 and CO_2 [27,61]. Therefore, such a modified electronic structure in Pd may lead to enhanced catalytic activity for FA dehydrogenation.

To further clarify the role of the metal/organic interface on the FA dehydrogenation activity, various interfaces including metal/C and metal/oxide interfaces were fabricated by growing $Cr_{0.4}Pd_{0.6}$ NPs on C, TiO_2, ZrO_2, SiO_2, CeO_2 and Al_2O_3. As shown in Fig. 4a-f, the $Cr_{0.4}Pd_{0.6}$ NPs supported on the above supports have the similar morphologies and average particle sizes as the $Cr_{0.4}Pd_{0.6}$ NPs in $Cr_{0.4}Pd_{0.6}$/M-β-CD-A catalyst. However, the catalytic activities of these $Cr_{0.4}Pd_{0.6}$ NPs supported on the above supports are clearly inferior to that of $Cr_{0.4}Pd_{0.6}$/M-β-CD-A catalysts (Fig. 4g-h), highlighting the role of metal/organic interface again. It has been demonstrated that the interactions between

the metal NPs and amine group are beneficial to the dehydrogenation of FA [62,63]. To understand the effect of the interactions between CrPd NPs and amine group in FA dehydrogenation activity, $Cr_{0.4}Pd_{0.6}$ NPs supported on various APTES-treated supports (C, TiO_2, ZrO_2, SiO_2, CeO_2 and Al_2O_3) were prepared and used as catalysts for FA dehydrogenation. The $Cr_{0.4}Pd_{0.6}$ NPs supported on these APTES-treated supports exhibit much lower catalytic activities than $Cr_{0.4}Pd_{0.6}$/M-β-CD-A (Fig. S10), indicating that the improved catalytic activity of the $Cr_{0.4}Pd_{0.6}$/M-β-CD-A can be mainly ascribed to the metal/organic interaction although the metal/amine-group interaction can more or less enhance the FA dehydrogenation activity. In addition, to determine whether or not Na^+ in M-β-CD-A accelerates the FA dehydrogenation, control experiment using HCOONa (0.02 mmol, which is equal to the amount of Na^+ in M-β-CD-A) over $Cr_{0.4}Pd_{0.6}/Al_2O_3$-A has been performed. The result shows that the presence of a small amount of HCOONa can not significantly promote the FA dehydrogenation (Fig. S11), suggesting that Na^+ in M-β-CD-A is not the key fact leading to the improved FA dehydrogenation activity.

The influence of the Cr/Pd ratio on the catalytic activity of the $Cr_{0.4}Pd_{0.6}$/M-β-CD-A catalyst for FA dehydrogenation was also investigated. Fig. 5a shows the catalytic activities of the Cr_xPd_{1-x}/M-β-CD-A ($0 \le x \le 1.0$) catalysts for FA dehydrogenation. It can be seen that the catalytic activity strongly depends on the Cr/Pd ratio. Despite Cr NPs are inactive for this reaction, the introduction of Cr drastically enhances the catalytic activity. The initial TOF of Cr_xPd_{1-x}/M-β-CD-A catalysts initially increases with increasing Cr content, showing the maximum initial TOF value of 5771 mol H_2 mol Pd^{-1} h^{-1} at $x = 0.4$ (Fig. 5b). However, further increase of the Cr content results in the decrease of activity. The enhanced catalytic activity is attributed to the electronic structure modulation of Pd active centers through a synergistic alloying effect between Pd and Cr, which has been testified by XPS spectra (Fig. S9). Moreover, the incorporation of Cr into the Pd structure greatly reduces the cost of the catalyst.

On the basis of the aforementioned results and previously reports [48,64], a plausible mechanism of FA dehydrogenation catalyzed by CrPd/M-β-CD-A has been proposed (Fig. 6). The electron donating amine groups, which acts as a proton scavenger, facilitates the O—H bond cleavage in FA molecule, leading to the formation of protonated amine. Meanwhile, the electron rich metal active center predominantly stabilizes the bridging formate species. Subsequently, the Pd-formate intermediate undergoes C–H bond dissociation to produce CO_2 and a metal-hydride. Finally, H_2 produced through the reaction of the hydride species with protonated amine, along with the regeneration of the active center.

Fig. S12 presents the catalytic decomposition kinetics profiles for FA dehydrogenation at various temperatures in the range of 303–333 K. The H_2 generation rate increases with the temperature rising. According to the Arrhenius plot, the activation energy (E_a) of $Cr_{0.4}Pd_{0.6}$/M-β-CD-A catalyst is calculated to be 49.4 kJ/mol, which is comparable to most of the previously reported heterogeneous catalysts for FA dehydrogenation (Table S2) [29,57,59]. The stability of the $Cr_{0.4}Pd_{0.6}$/M-β-CD-A catalyst was also investigated by adding the same amount of FA into the reactor after the completion of the previous run. As shown in Fig. S13, there is a slight decrease in the activity after three cycles. Moreover, the $Cr_{0.4}Pd_{0.6}$/M-β-CD-A after the stability test was characterized by TEM, showing that there is no noticeable change in the size after three cycles (Fig. S14), indicating the excellent stability of our $Cr_{0.4}Pd_{0.6}$/M-β-CD-A catalyst.

4. Conclusions

In conclusion, we have demonstrated that metal/organic interfaces offer an effective strategy to control the particle size, distribution and electronic structure of NPs to optimize their catalytic activities for FA dehydrogenation for H_2 production. The $Cr_{0.4}Pd_{0.6}$/M-β-CD-A catalyst exhibits excellent activity and 100% H_2 selectivity with an initial TOF as high as 5771 mol H_2 mol Pd^{-1} h^{-1} without any additive at 323 K, making it one of the most active heterogeneous catalysts for this reaction. This work not only opens up an avenue to develop low cost and highly efficient heterogeneous catalysts for FA dehydrogenation, but also provides a simple strategy to synthesize a wide series of metal/organic interface heterogeneous catalysts for energy and environment related chemical and electrochemical reactions.

Acknowledgements

This work was supported by National Natural Science Foundation of China (51601018, 51608050, 51671035); Jilin Province Science and Technology Development Project (20170520122JH); and Science and Technology Research Project of the Education Department of Jilin Province (JJKH20170549KJ).

Appendix A. Supplementary data

Supplementary material related to this article can be found, in the online version, at doi:https://doi.org/10.1016/j.apcatb.2019.117776.

References

[1] L. Schlapbach, A. Zttel, Nature 414 (2001) 353–358.
[2] A. Boddien, H. Junge, Nat. Nanotechnol. 6 (2011) 265–266.
[3] X. Xu, Y. Chen, W. Zhou, Z. Zhu, C. Su, M. Liu, Z. Shao, Adv. Mater. 28 (2016) 6442–6448.
[4] H. Dai, B. Xia, L. Wen, C. Du, J. Su, W. Luo, G. Cheng, Appl. Catal. B: Environ. 165 (2015) 57–62.
[5] S. Fukuzumi, T. Kobayashi, T. Suenobu, J. Am. Chem. Soc. 132 (2010) 1496–1497.
[6] B. Loges, A. Boddien, H. Junge, M. Beller, Angew. Chem. Int. Ed. 47 (2008) 3962–3965.
[7] A. Boddien, D. Mellmann, F. Gärtner, R. Jackstell, H. Junge, P.J. Dyson, G. Laurenczy, R. Ludwig, M. Beller, Science 333 (2011) 1733–1736.
[8] Z. Li, Q. Xu, Acc. Chem. Res. 50 (2017) 1449–1458.
[9] S. Jones, J. Qu, K. Tedsree, X.Q. Gong, S.C.E. Tsang, Angew. Chem. 124 (2012) 11437–11440.
[10] Q.L. Zhu, N. Tsumori, Q. Xu, J. Am. Chem. Soc. 137 (2015) 11743–11748.
[11] X. Gu, Z.H. Lu, H.L. Jiang, T. Akita, Q. Xu, J. Am. Chem. Soc. 133 (2011) 11822–11825.
[12] Z. Wang, J. Yan, Y. Ping, H. Wang, W. Zheng, Q. Jiang, Angew. Chem. Int. Ed. 52 (2013) 4406–4409.
[13] P. Zhao, W. Xu, D. Yang, W. Luo, G. Cheng, ChemistrySelect 1 (2016) 1400–1404.
[14] Z.L. Wang, Y. Ping, J.M. Yan, H.L. Wang, Q. Jiang, Int. J. Hydrogen Energy 39 (2014) 4850–4856.
[15] M. Cargnello, V.V.T.D. Nguyen, T.R. Gordon, R.E. Diaz, E.A. Stach, R.J. Gorte, P. Fornasiero, C.B. Murray, Science 341 (2013) 771–773.
[16] W. Zhan, Q. He, X. Liu, Y. Guo, Y. Wang, L. Wang, Y. Guo, A.Y. Borisevich, J. Zhang, G. Lu, S. Dai, J. Am. Chem. Soc. 138 (2016) 16130–16139.
[17] G. Chen, Y. Zhao, G. Fu, P.N. Duchesne, L. Gu, Y. Zheng, X. Weng, M. Chen, P. Zhang, C.W. Pao, J.F. Lee, N. Zheng, Science 344 (2014) 495–499.
[18] D. Gao, Y. Zhang, Z. Zhou, F. Cai, X. Zhao, W. Huang, Y. Li, J. Zhu, P. Liu, F. Yang, G. Wang, X. Bao, J. Am. Chem. Soc. 139 (2017) 5652–5655.
[19] Q. Bi, X. Du, Y. Liu, Y. Cao, H. He, K. Fan, J. Am. Chem. Soc. 134 (2012) 8926–8933.
[20] F. Song, Q. Zhu, X. Yang, W. Zhan, P. Pachfule, N. Tsumori, Q. Xu, Adv. Energy Mater. 8 (2018) 1701416.
[21] A. Bulut, M. Yurderi, M. Kaya, M. Aydemir, A. Baysal, F. Durap, M. Zahmakiran, New J. Chem. 42 (2018) 16103–16114.
[22] N. Caner, A. Bulut, M. Yurderi, I.E. Ertas, H. Kivrak, M. Kaya, M. Zahmakiran, Appl. Catal. B: Environ. 210 (2017) 470–483.
[23] Y. Karatas, A. Bulut, M. Yurderi, I.E. Ertas, O. Alal, M. Gulcan, M. Celebi, H. Kivrak, M. Kaya, M. Zahmakiran, Appl. Catal. B: Environ. 180 (2016) 586–595.
[24] A. Bulut, M. Yurderi, Y. Karatas, Z. Say, H. Kivrak, M. Kaya, M. Gulcan, E. Ozensoy, M. Zahmakiran, ACS Catal. 5 (2015) 6099–6110.
[25] M. Yurderi, A. Bulut, N. Caner, M. Celebi, M. Kaya, M. Zahmakiran, Chem. Commun. 51 (2015) 11417–11420.
[26] M. Yurderi, A. Bulut, M. Zahmakiran, M. Kaya, Appl. Catal. B: Environ. 160-161 (2014) 514–524.
[27] K. Tedsree, T. Li, S. Jones, C.W.A. Chan, K.M.K. Yu, P.A.J. Bagot, E.A. Marquis, G.D.W. Smith, S.C.E. Tsang, Nat. Nanotechnol. 6 (2011) 302–307.
[28] Z. Zhang, S. Cao, Y. Liao, C. Xue, Appl. Catal. B: Environ. 162 (2015) 204–209.
[29] Q. Bi, J. Lin, Y. Liu, H. He, F. Huang, Y. Cao, Angew. Chem. Int. Ed. 55 (2016) 11849–11853.
[30] Z. Li, X. Yang, N. Tsumori, Z. Liu, Y. Himeda, T. Autrey, Q. Xu, ACS Catal. 7 (2017) 2720–2724.
[31] Q. Wang, N. Tsumori, M. Kitta, Q. Xu, ACS Catal. 8 (2018) 12041–12045.
[32] B. Wu, N. Zheng, Nano Today 8 (2013) 168–197.
[33] B. Wu, H. Huang, J. Yang, N. Zheng, G. Fu, Angew. Chem. Int. Ed. 51 (2012)

3440–3443.
[34] T. Xue, Z. Lin, C.Y. Chiu, Y. Li, L. Ruan, G. Wang, Z. Zhao, C. Lee, X. Duan, Y. Huang, Sci. Adv. 3 (2017) 1600615.
[35] G. Chen, C. Xu, Xi. Huang, J. Ye, L. Gu, G. Li, Z. Tang, B. Wu, H. Yang, Z. Zhao, Z. Zhou, G. Fu, N. Zheng, Nat. Mater. 15 (2016) 564–569.
[36] Z. Cao, D. Kim, D. Hong, Y. Yu, J. Xu, S. Lin, X. Wen, E.M. Nichols, K. Jeong, J.A. Reimer, P. Yang, C.J. Chang, J. Am. Chem. Soc. 138 (2016) 8120–8125.
[37] G. Zhu, P. Gai, L. Wu, J. Zhang, X. Zhang, J. Chen, Chem.-Asian J. 7 (2012) 732–737.
[38] S. Sakthinathan, S. Kubendhiran, S. Chen, P. Sireesha, C. Karuppiah, C. Su, Electroanalysis 29 (2017) 587–594.
[39] D. Murphy, M.N. de Pinho, J. Membr. Sci. 106 (1995) 245–257.
[40] Y. Zhang, F. Jiang, D. Huang, S. Hou, H. Wang, M. Wang, Y. Chi, Z. Zhao, RSC Adv. 8 (2018) 31348–31357.
[41] B.S. Holla, M. Mahalinga, B. Poojary, M. Ashok, P.M. Akberali, Indian J. Chem., Sect. B: Org. Chem. Incl. Med. Chem. 45 (2006) 568–571.
[42] S. Davaran, J. Hanaee, A. Khosravi, J. Control. Release 58 (1999) 279–287.
[43] L. Wang, S. Dong, Z. Zhang, Y. Wang, X. Zhang, X. Zhang, P. Zhang, L. Zhao, Se pu 34 (2016) 89–95.
[44] D.W. Gao, Z.L. Wang, C. Wang, L.Y. Wang, Y. Chi, M.G. Wang, J.J. Zhang, C. Wu, Y. Gu, H.L. Wang, Z.K. Zhao, Chem. Eng. J. 361 (2019) 953–959.
[45] Z. Wang, J. Yan, H. Wang, Y. Ping, Q. Jiang, Sci. Rep. 2 (2012) 598.
[46] S. Guo, S. Zhang, X. Sun, S. Sun, J. Am. Chem. Soc. 133 (2011) 15354–15357.
[47] H. Yin, S. Liu, C. Zhang, J. Bao, Y. Zheng, M. Han, Z. Dai, ACS Appl. Mater. Interfaces 6 (2014) 2086–2094.
[48] J. Cheng, X. Gu, P. Liu, T. Wang, H. Su, J. Mater. Chem. A 4 (2016) 16645–16652.
[49] Z.L. Wang, J.M. Yan, H.L. Wang, Y. Ping, Q. Jiang, J. Mater. Chem. A 1 (2013) 12721–12725.
[50] O. Metin, X. Sun, S. Sun, Nanoscale 5 (2013) 910–912.
[51] S. Zhang, Ö. Metin, D. Su, S. Sun, Angew. Chem. Int. Ed. 52 (2013) 3681–3684.
[52] J.M. Yan, S.J. Li, S.S. Yi, B.R. Wulan, W.T. Zheng, Q. Jiang, Adv. Mater. 30 (2018) 1703038.
[53] L. Yang, X. Hua, J. Su, W. Luo, S. Chen, G. Cheng, Appl. Catal. B: Environ. 168-169 (2015) 423–428.
[54] J. Cheng, X. Gu, X. Sheng, P. Liu, H. Su, J. Mater. Chem. A 4 (2016) 1887–1894.
[55] K. Jiang, K. Xu, S. Zou, W.B. Cai, J. Am. Chem. Soc. 136 (2014) 4861–4864.
[56] T. Feng, J.M. Wang, S.T. Gao, C. Feng, N.Z. Shang, C. Wang, L.L. Xue, Appl. Surf. Sci. 469 (2019) 431–436.
[57] Y. Chen, Q.L. Zhu, N. Tsumori, Q. Xu, J. Am. Chem. Soc. 137 (2015) 106–109.
[58] N. Wang, Q. Sun, R. Bai, X. Li, G. Guo, J. Yu, J. Am. Chem. Soc. 138 (2016) 7484–7487.
[59] F.Z. Song, Q.L. Zhu, N. Tsumori, Q. Xu, ACS Catal. 5 (2015) 5141–5144.
[60] J.M. Yan, Z.L. Wang, L. Gu, S.J. Li, H.L. Wang, W.T. Zheng, Q. Jiang, Adv. Energy Mater. 5 (2015) 1500107.
[61] J. Cheng, X. Gu, P. Liu, H. Zhang, L. Ma, Su H, Appl. Catal. B: Environ. 218 (2017) 460–469.
[62] M. Yadav, T. Akita, N. Tsumoria, Q. Xu, J. Mater. Chem. 22 (2012) 12582–12586.
[63] A. Bulut, M. Yurderi, Y. Karatas, M. Zahmakiran, H. Kivrak, M. Gulcan, M. Kaya, Appl. Catal. B: Environ. 164 (2015) 324–333.
[64] K. Mori, K. Naka, S. Masuda, K. Miyawaki, H. Yamashita, ChemCatChem 9 (2017) 3456–3462.